



Di-lepton production in p+p collisions at $\sqrt{s_{NN}} = 200$ GeV from STAR

Lijuan Ruan (for the STAR Collaboration)

Physics Department, Brookhaven National Laboratory, Upton NY 11973

Abstract

The di-electron analysis for 200 GeV p+p collisions is presented in this article. The cocktail simulations of di-electrons from light flavor meson decays and heavy flavor decays are reported and compared with data. The perspectives for di-lepton measurements in Au+Au collisions are discussed.

Keywords: di-electron continuum, cocktail simulations, 200 GeV p+p collisions

1. Introduction

Ultra-relativistic heavy ion collisions provide a unique environment to study properties of strongly interacting matter at high temperature and high energy density [1]. One of the crucial probes of this strongly interacting matter are di-lepton measurements in the low and intermediate mass region. Di-leptons are not affected by the strong interaction once produced, therefore they can probe the whole evolution of the collision. The di-lepton spectra in the intermediate mass range ($1.1 < M_{ll} < 3.0$ GeV/ c^2) are directly related to thermal radiation of the QGP [2, 3]. In the low mass range ($M_{ll} < 1.1$ GeV/ c^2), we can study vector meson in-medium properties through their di-lepton decays, where any modifications observed may relate to the possibility of chiral symmetry restoration. Measurements in p+p collisions provide a crucial reference for the corresponding measurements in heavy ion collisions. At STAR, the newly installed Time-of-Flight detector (TOF) offers high acceptance and efficiency [4]. The TOF, combined with measurements of ionization energy loss (dE/dx) from the Time Projection Chamber (TPC) [5], enables electron identification (eID) with high purity from low to intermediate p_T [6]. In this article we present the di-lepton continuum from 200 GeV p+p collisions carried out in 2009. We utilized eID from the TOF and TPC. The cocktail simulations are presented and compared to the data. Finally, future capabilities for di-lepton measurements at STAR in Au+Au collisions are discussed.

2. Data Analysis and Results

At STAR [7], there are three detectors which are used for electron identification at mid-rapidity: the TPC, the TOF, and the Barrel Electron-magnetic Calorimeter (BEMC) [8]. The TPC is the main tracking detector at STAR, measuring momenta and path-lengths of particles created in the collisions. The dE/dx is used for particle identification [9, 10]. The full TOF system was installed in STAR in year 2009 and extends $\pi(K)$ identification up to 1.6 GeV/ c and $p(\bar{p})$ up to 3 GeV/ c [11, 12]. By combining the velocity (β) information from the TOF and the dE/dx from the TPC, electrons can be clearly identified from low to intermediate p_T . In addition, the EMC is used for triggering high energy photons and electrons based on the energy deposited in the detector.

In Run 9 p+p collisions, the TOF azimuthal acceptance is 72% at $|\eta| < 0.9$. In the di-electron analysis, we used 107 million minimum-bias p+p events at $\sqrt{s_{NN}} = 200$ GeV. The collision vertex was required to be within 50 cm from

TPC center along the beam line. We selected electron candidates with a 99% purity by applying velocity and dE/dx cuts on tracks with $p_T > 0.2$ GeV/ c . The velocity was required to be in the range of $|1/\beta - 1| < 0.03$. The dE/dx cut is p_T dependent to ensure electrons have a 99% purity in each p_T bin. The e^+ and e^- pairs from the same events were combined to reconstruct the invariant mass distributions (M_{ee}) marked as unlike-sign distributions which contain both signal and background. Two methods were used for background reconstruction, like-sign and mixed-event techniques. In the like-sign technique, the electron pairs with the same charge sign were reconstructed from the same events. In the mixed-event technique used in this analysis, unlike-sign pairs were reconstructed from different events. In order to ensure the mixed events have similar acceptances, we only mixed events which had collision vertices within 5 cm of each other in the beam line direction. The background pairs were formed from two tracks in different events.

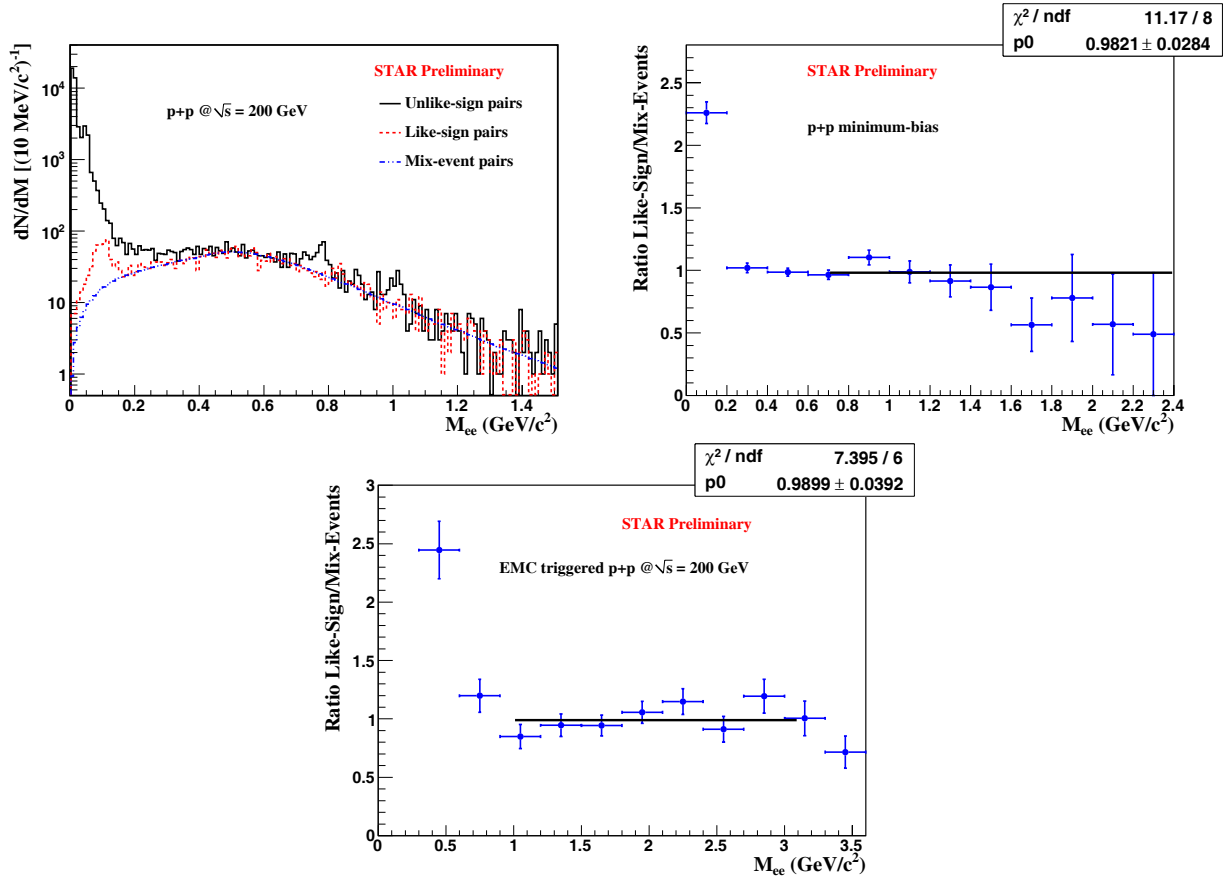


Figure 1: (top-left panel) The electron pair invariant mass distributions for unlike-sign pairs, like-sign, and mixed-event background in minimum-bias p+p collisions. (top-right panel) The ratio of like-sign over mixed-event distributions in minimum-bias p+p collisions. (bottom panel) The ratio of like-sign over mixed-event distributions in EMC triggered p+p collisions.

2.1. Background subtraction

Figure 1 (top-left panel) shows the invariant mass distribution for unlike-sign pairs, like-sign, and mixed-event background. The mixed-event distribution was normalized by a constant to the like-sign distribution in the mass region of 0.4–1.5 GeV/c^2 . In the low mass region, there is correlated cross pair background, which comes from double Dalitz decays, Dalitz decays followed by a conversion of the decay photon, or two-photon decays followed by conversion of both photons. This background is included in the like-sign distribution but not in the mixed-event background. At $M_{ee} < 0.7$ GeV/c^2 , the like-sign distribution was used for background subtraction. At higher mass, we compared the shape of like-sign and mixed-event distributions and found they matched reasonably well, as shown in the ratio plot in Fig. 1 (top-right panel). A constant was used to fit the ratio of like-sign over mixed-event distributions

and the χ^2/NDF is about 1 [13]. We did the same exercise using EMC triggered events for di-electron analysis, in which one electron is required to trigger the EMC and has a transverse momentum greater than 2 GeV/c, and the p_T of the other electron is greater than 0.2 GeV/c. We found that with a significantly higher transverse momentum for the pair, the shape of like-sign over mixed-event distributions matched in the mass region of 1-3 GeV/c², as shown in the ratio plot in Fig. 1 (bottom panel). This indicates that the jet contribution within the STAR acceptance does not significantly alter the combinatorial background shape in the mixed-event method and is negligible given our precision. PYTHIA simulations with jets are on-going. For minimum-bias events, at $M_{ee} > 0.7$ GeV/c², we subtracted the normalized mixed-event background. The di-electron continuum after background subtraction is shown in Fig. 2 (right panel). The errors shown are statistical only. The systematic uncertainties on the normalization and background subtraction are still under study. In the future, more simulation will be done to further study background subtraction at $M_{ee} > 0.7$ GeV/c².

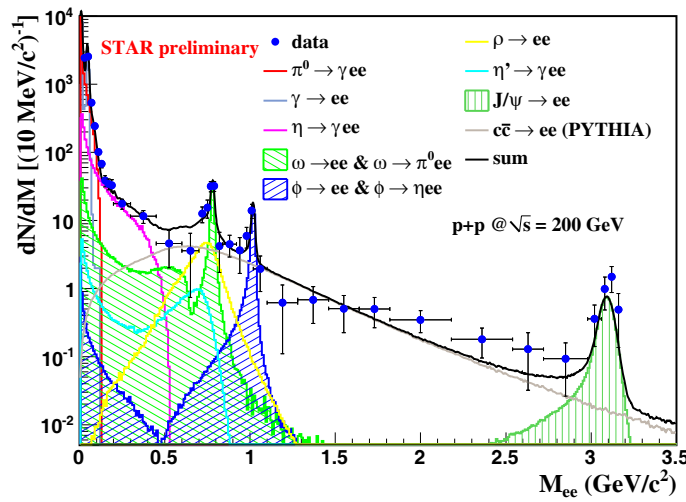


Figure 2: The comparison for di-electron continuum between data and simulation in 200 GeV minimum-bias p+p collisions. The di-electron continuum from simulations with different source contributions are also shown.

2.2. Cocktail simulation

The di-electron signals may come from light flavor hadron decays and heavy flavor hadron decays, for example, π^0 , η , and η' Dalitz decays: $\pi^0 \rightarrow \gamma e^+ e^-$, $\eta \rightarrow \gamma e^+ e^-$, and $\eta' \rightarrow \gamma e^+ e^-$; vector meson decays: $\omega \rightarrow \pi^0 e^+ e^-$, $\omega \rightarrow e^+ e^-$, $\rho^0 \rightarrow e^+ e^-$, $\phi \rightarrow \eta e^+ e^-$, $\phi \rightarrow e^+ e^-$, and $J/\psi \rightarrow e^+ e^-$; heavy flavor decays: $c\bar{c} \rightarrow e^+ e^-$ and $b\bar{b} \rightarrow e^+ e^-$; and Drell-Yan contributions. We fit the invariant yields of measured mesons with the Tsallis blast-wave functions [14], used the Tsallis functions as our inputs, and decayed them into di-electrons with GEANT using STAR year 2009 geometry. The electron candidates were reconstructed as tracks. We applied the same cuts for the electron tracks as in the data and generated the $e^+ e^-$ cocktails from different contribution sources for the same number of events and rapidity ranges as used in the data analysis. The gamma conversion $\gamma \rightarrow e^+ e^-$ was not rejected and its contribution to di-electron continuum was simulated with the same method. Compared to what was presented in the conference, the Dalitz decays of $\omega \rightarrow \pi^0 e^+ e^-$ and $\eta' \rightarrow \gamma e^+ e^-$ were updated using the correct Kroll-Wada expression [15]; and the $\rho^0 \rightarrow e^+ e^-$ line shape was updated with the Boltzmann phase space factor [16, 17]. The total contribution from the simulation is shown as the black solid curve on Fig. 2 and is found to be consistent with data. It is also consistent with what was shown in the conference. The invariant yield of π^0 is taken as the average of π^+ and π^- [12, 18]. The yields of ϕ [19] and ρ^0 [17] are from STAR while η [20], ω [21] and J/ψ [22] are from PHENIX. In this simulation, the $c\bar{c}$ cross section was an input and constrained by the measurement from STAR [6, 23]. In the intermediate mass region, di-electron continuum is dominated by the $c\bar{c}$ contribution. The χ^2/NDF of the comparison between data and simulation is 36/30 in the mass region of 0.1-3.2 GeV/c². The uncertainties on the cocktail including the decay form factors, the measured cross section for each hadron, and the efficiency uncertainties are under-study. The current precision

of STAR di-electron data presented here does not allow us to distinguish STAR's measured charm cross section from PHENIX's [6, 24]. With D meson reconstruction and non-photon electron measurements at low p_T from the TPC and TOF from year 2009 p+p collisions, the charm cross section will be measured with a better precision at STAR and can be used to further constrain the charm correlation contribution to the di-electron continuum measurements.

2.3. Future measurements in Au+Au collisions

In year 2010, STAR has taken a few hundred million minimum-bias events in 200, 62, and 39 GeV Au+Au collisions with full TOF azimuthal coverage and low conversion material budget, which will enable us to study the following physics topics: 1) di-electron enhancement in the low mass region [25]; 2) in-medium modifications of vector meson decays; 3) virtual photons [26]; 4) $c\bar{c}$ medium modifications; and 5) possible thermal radiation in the intermediate mass region. With the current data sets, it will be difficult to measure 4) or 5) since they are coupled to each other and one is the other's background for the physics case. So far at RHIC, there is no clear answer about thermal radiation in the intermediate mass region. The future detector upgrade with the Heavy Flavor Tracker at STAR will provide precise charm cross section measurements [27], however the measurements of $c\bar{c}$ correlations will still be challenging if not impossible. An independent approach is proposed with the proposed Muon Telescope Detector [28], $\mu - e$ correlations, to measure the contribution from heavy flavor correlations to the di-electron or di-muon continuum. This will make it possible to access the thermal radiation in the intermediate mass region.

2.4. Summary

In summary, the di-electron continuum is measured in 200 GeV p+p collisions at STAR. The cocktail simulations are consistent with the data in 200 GeV p+p collisions, providing a reference for the future Au+Au study. The newly installed TOF system enables this study and will also provide interesting physics outputs with the data taken in year 2010 in Au+Au collisions at different beam energies.

References

- [1] J. Adams *et al.*, Nucl. Phys. A **757**, 102 (2005).
- [2] R. Rapp and J. Wambach, Adv. Nucl. Phys. **25** (2000) 1.
- [3] Electromagnetic Probes at RHIC II (Working Group Report), G. David, R. Rapp and Z. Xu, Phys. Rept. **462**, 176 (2008).
- [4] B. Bonner *et al.*, Nucl. Instr. Meth. A **508**, 181 (2003); M. Shao *et al.*, Nucl. Instr. Meth. A **492**, 344 (2002); J. Wu *et al.*, Nucl. Instr. Meth. A **538**, 243 (2005).
- [5] M. Anderson *et al.*, Nucl. Instr. Meth. A **499**, 659 (2003).
- [6] J. Adams *et al.*, Phys. Rev. Lett. **94**, 062301 (2005).
- [7] K. H. Ackermann *et al.*, Nucl. Instr. Meth. A **499**, 624 (2003).
- [8] M. Beddo *et al.*, Nucl. Instr. Meth. A **499**, 725 (2003).
- [9] H. Bichsel, Nucl. Instr. Meth. A **562**, 154 (2006).
- [10] Y. Xu *et al.*, Nucl. Instr. Meth. A **614**, 28 (2010).
- [11] M. Shao *et al.*, Nucl. Instr. Meth. A **558**, 419 (2006).
- [12] J. Adams *et al.*, Phys. Lett. B **616**, 8 (2005).
- [13] A. Adare *et al.*, Phys. Rev. C **81**, 034911 (2010).
- [14] Z. Tang *et al.*, Phys. Rev. C **79**, 051901 (2009); M. Shao *et al.*, J. Phys. G **37**, 085104 (2010).
- [15] N. M. Kroll and W. Wada, Phys. Rev. **98**, 1355 (1955).
- [16] R. Rapp, Nucl. Phys. A **725**, 254 (2003); E. V. Shuryak and G. Brown, Nucl. Phys. A **717**, 322 (2003).
- [17] J. Adams *et al.*, Phys. Rev. Lett. **92**, 092301 (2004).
- [18] J. Adams *et al.*, Phys. Lett. B **637**, 161 (2006).
- [19] J. Adams *et al.*, Phys. Lett. B **612**, 181 (2005).
- [20] S.S. Adler *et al.*, Phys. Rev. C **75**, 024909 (2007).
- [21] S.S. Adler *et al.*, Phys. Rev. C **75**, 051902 (2007).
- [22] A. Adare *et al.*, Phys. Rev. Lett. **98**, 232002 (2007).
- [23] W. Xie *et al.*, for the STAR Collaboration, these proceedings.
- [24] A. Adare *et al.*, Phys. Rev. Lett. **97**, 252002 (2006).
- [25] S. Afanasiev *et al.*, nucl-ex/0706.3034.
- [26] A. Adare *et al.*, Phys. Rev. Lett. **104**, 132301 (2010).
- [27] STAR Heavy Flavor Tracker proposal, http://rnc.lbl.gov/hft/docs/hft_final_submission_version.pdf; S. Kleinfelder *et al.*, Nucl. Instr. Meth. A **565**, 132 (2006).
- [28] STAR Muon Telescope Detector Proposal: http://drupal.star.bnl.gov/STAR/system/files/MTD_proposal_v14.pdf; Z. Xu, BNL LDRD project 07-007; L. Ruan *et al.*, J. Phys. G **36**, 095001 (2009); Y. Sun *et al.*, Nucl. Instr. Meth. A **593**, 307 (2008).